

Exact Medial Axis Computation for Triangulated Solids with Respect to Piecewise Linear Metrics

Oswin Aichholzer¹, Wolfgang Aigner¹, Franz Aurenhammer², and Bert Jüttler³

¹ Institute for Software Technology, Graz University of Technology, Austria

² Institute for Theoretical Computer Science, Graz University of Technology, Austria

³ Institute of Applied Geometry, Johannes Kepler University Linz, Austria

Abstract. We propose a novel approach for the medial axis approximation of triangulated solids by using a polyhedral unit ball B instead of the standard Euclidean unit ball. By this means we compute the exact medial axis $\text{MA}(\Omega)$ of a triangulated solid Ω with respect to a piecewise linear (quasi-) metric d_B . The obtained representation of Ω by the medial axis transform $\text{MAT}(\Omega)$ allows for a convenient computation of the trimmed offset of Ω with respect to d_B . All calculations are performed within the field of rational numbers, resulting in a robust and efficient implementation of our approach. Adapting the properties of B provides an easy way to control the level of details captured by the medial axis, making use of the implicit pruning at flat boundary features.

Keywords: medial axis, piecewise linear metric, mesh boundary, trimmed offset

1 Introduction

The medial axis is a skeleton-like structure, capturing the features of a shape in a lower-dimensional configuration. It has originally been introduced by Blum [7] for matters of shape representation, and has proved to be useful for various applications such as shape recognition, robot motion, finite element mesh generation [17], and offset computation. The computation of the exact medial axis – or of an approximation thereof – is a popular task in computational geometry and geometric computing. The huge variety of publications addressing different boundary representations [13, 14, 20], pruning techniques [9, 22] and applications [8, 12] is remarkable. See also [5] for a state of the art survey in this area. In the case of polyhedral objects, there exist numerical tracing techniques [24] (which have recently been extended to objects with curved boundaries [23]) and methods based on spatial decompositions [16, 21].

For boundaries represented by dense point sets, it is a common approach to derive a medial axis approximation by isolating a subset of its Voronoi diagram [14]. The algorithm relies on heavy pruning and has (depending on the denseness of the point set) problems with capturing sharp features. Another approximating structure, that also allows to deal with non-exact boundaries, is the

scale axis [22], based on a ball-representation of the shape. Pruning is achieved by careful scaling of the balls, which, on the downside, can lead to the introduction of topologically incorrect fragments. Both of these methods work in 2D and 3D, but they do not constitute an exact representation of a shape. They are thus suited for shape recognition and comparison but not for offset computation.

Exact medial axis computation relies on an exact boundary representation, and is well examined for piecewise smooth boundaries in 2-space. For straight-line polygons Lee [20] introduced an intuitive $O(n \log n)$ algorithm, which was later improved to an optimal (yet unimplemented) linear-time algorithm [11]. For circular arc boundaries a full implementation of a randomized algorithm (with expected $O(n \log n)$ computing time) is provided in [2]. To the contrary, it has turned out that in the three dimensional space the exact medial axis computation, even for shapes with piecewise linear boundaries, is a rather challenging problem. Here difficulties arise from the combinatorial complexity of the medial axis, as well as the high algebraic degree of its components. Especially the latter leads, due to the necessity of an algebraic kernel, to computing time and representation issues. So far, the only work in this context that provides a full implementation and some computing times is by Culver et al. [13], introducing complex algebraic algorithms to deal with the above-mentioned problems.

In this work we provide an approach that computes the exact medial axis of a triangulated solid (i.e., a solid object whose boundary surface is a triangular mesh) with respect to a piecewise linear quasi-metric d_B [26] induced by a convex polyhedral unit ball B (see also Minkowski functionals [19]). While the use of more general convex distance functions for bisector and Voronoi computation is no novelty [10, 18], these generalized distances, however, have not been used for medial axis computations so far. This is quite surprising, considering that for given rational data (rational coordinates of mesh and unit ball vertices) the resulting linearity of the structure allows all computations to be performed within the field of rational numbers. We took advantage of this, providing a robust and stable implementation of the algorithm.

The quasi-metric d_B induces a piecewise linear medial axis transform $\text{MAT}(\Omega)$, which describes the shape Ω fully and exactly, see Fig. 1a for an example. In order to deal with the structural complexity of the medial axis in 3D, we introduce planar contact arrangements, one for each possible contact between the components of the unit ball B and the boundary, respectively (see Sections 3 and 4). After computing these arrangements, we are able to calculate the components of the medial axis with respect to the quasi-metric d_B . In this way we reduce the problem of medial axis construction in 3D to a number of two dimensional problems.

The use of polyhedral unit balls permits interesting operations such as implicit pruning, resulting in pseudo-seams which will be introduced in Section 2. This allows us to influence the structure and complexity of the medial axis by varying combinatorial and geometrical properties of the unit ball. Furthermore, we will show that our representation via $\text{MAT}(\Omega)$ is very convenient to compute trimmed offsets with respect to d_B , see Fig. 1b (see Section 5.2 for details). In

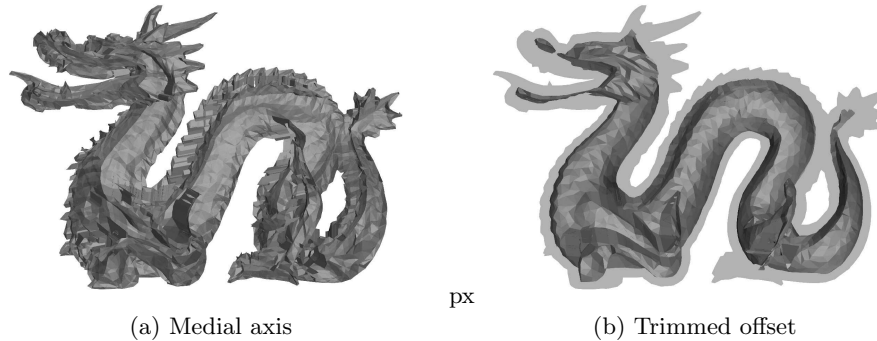


Fig. 1: Piecewise linear medial axis approximation and trimmed offset for a dragon mesh with 12,000 faces, using a quasi-metric defined by a tetrahedral unit ball.

Section 6 we will describe the close relation between the medial axes $MA(\Omega)$ induced by Euclidean and polyhedral unit balls. This also identifies $MA(\Omega)$ with respect to a piecewise linear metric d_B as an approximation of the Euclidean medial axis, where the quality of the approximation depends on the chosen unit ball B .

2 Preliminaries

Throughout this paper we consider an open set Ω in \mathbb{R}^d ($d = 2, 3$) with a piecewise linear boundary $\partial\Omega$. We moreover assume that the boundary is triangulated and consists of edges, vertices, and triangular facets (the latter ones only for $d = 3$). We shall refer to Ω as a *triangulated solid*.

2.1 Unit balls and metrics

Let B be a bounded, open and convex set in \mathbb{R}^d which contains the origin o . In particular, we are interested in two cases.

- (E) B may be the usual *Euclidean unit ball*, $B = \{x : \|x\| < 1\} \subset \mathbb{R}^d$.
- (L) B may be the interior of a *convex polyhedron*, i.e., the boundary ∂B is piecewise linear. Similar to $\partial\Omega$ we assume that ∂B is given by a triangulation.

In the second case (L) we shall assume that no edge or facet of ∂B is parallel to any edge or facet of $\partial\Omega$, i.e., we assume that Ω is in *general position* with respect to B . Later we will specify additional conditions that we assume to be satisfied.

By these assumptions it is guaranteed that a component of ∂B and a component of $\partial\Omega$ intersect in at most one point. To achieve this, a slight perturbation of the boundary of B and/or Ω – e.g. by application of the Simulation-of-Simplicity (SOS) technique [15] – can be applied. Clearly, by restricting the perturbation

to the vertices of B we can even keep the original domain unchanged. However, even if perturbations are applied to the vertices of a triangulated solid, the resulting changes in the medial axis are not dramatic, provided that convex edges are not made reflex or vice versa.

For any points x and y , let r be the ray from x through y and B^* the body B translated by \vec{ox} . There exists a unique intersection point v of ∂B^* and r . The distance function

$$d_B(x, y) := \frac{\|y - x\|}{\|v - x\|} \quad (1)$$

defines a *quasi-metric* [26], meaning that d_B is positive definite and fulfills the triangle inequality, but is not necessarily symmetric. The given convex body B is the *unit ball* with respect to the quasi-metric.

If B is centrally symmetric with respect to the origin o , then d_B is a *metric*. In particular, the first choice of B as the Euclidean unit ball gives the usual Euclidean metric.

2.2 Maximal and almost maximal balls

In the remainder of this paper we will use the symbols B' , B'' etc. to represent convex polyhedra which are obtained from B by applying restricted Euclidean similarity transformations consisting of a *scaling* combined with a *translation*, but no rotation. Clearly, these convex sets are *balls* with respect to the quasi-metric defined by B , since they consist of all points whose distance d_B from the translated origin does not exceed the scaling factor.

Definition 1 A ball B' is said to be a *maximal ball* associated with the triangulated solid Ω if

1. it is contained in Ω , $B' \subseteq \Omega$, and if
2. any other ball B'' satisfying $B' \subset B''$ is not contained in Ω , i.e., $B'' \not\subseteq \Omega$.

Moreover, the ball B' is called an *almost maximal ball* associated with Ω , if it is contained in Ω and the boundary $\partial B'$ shares at least two points with $\partial\Omega$.

In the Euclidean case (E), the two notions are equivalent. In the case (L) of a piecewise linear metric, however, there may exist almost maximal balls which are not maximal.

2.3 Types of contact

In this section we consider exclusively the case (L) of a piecewise linear metric.

If we consider a two-dimensional domain Ω in the plane, the following types of contact between $\partial\Omega$ and the boundaries $\partial B'$ of almost maximal balls are possible:

1. A vertex of $\partial\Omega$ is in contact with an edge of $\partial B'$, and
2. an edge or vertex of $\partial\Omega$ is in contact with a vertex of $\partial B'$.

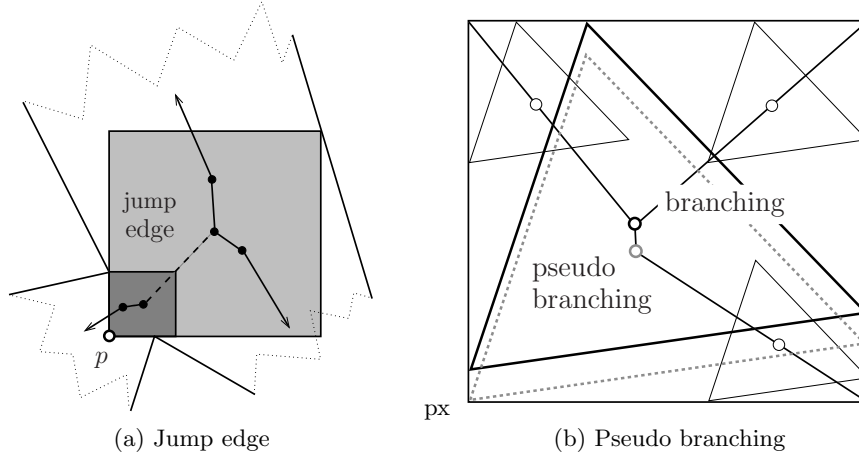


Fig. 2: (a) 2D example of a jump edge with center of scaling p . (b) A triangular unit ball induces a pseudo-branching in the medial axis of a square domain.

We will exclude the case where an almost maximal ball possesses two contacts of the first type that are realized at *only one edge* of $\partial B'$, by requiring that no edge of ∂B is parallel to any line connecting any two vertices of $\partial\Omega$. (It suffices to assume that this condition is satisfied by all pairs of non-convex vertices of $\partial\Omega$.) This is subsumed by the fact that we assume B and Ω to be in *general position*. We shall see later that almost maximal balls of this type would correspond to two-dimensional components of the medial axis.

Consider an almost maximal ball B' that possesses exactly two contacts which are of the first type and realized in the interior of two *neighboring* edges of $\partial B'$, and let p be the common vertex of the neighboring edges. In this case, any uniform scaling with a factor f sufficiently close to 1 and center p transforms B' into another almost maximal ball which is either a subset (if $f < 1$) or a super-set (if $f > 1$) of B' , see Fig. 2a.

The same phenomenon occurs if an almost maximal ball B' possesses contacts of the first and the second type, and the contact vertex of $\partial B'$ is a segment end point of the contact edge of $\partial B'$.

In the three-dimensional case, the following types of contact between $\partial\Omega$ and the boundaries $\partial B'$ of almost maximal balls are possible:

1. A vertex of $\partial\Omega$ is in contact with a facet of $\partial B'$,
2. a vertex or an edge of $\partial\Omega$ is in contact with an edge of $\partial B'$, and
3. a vertex, an edge or a facet of $\partial\Omega$ is in contact with a vertex of $\partial B'$.

Again we exclude the case of almost maximal balls with two contacts of the first type which are realized in the interior of *only one facet* of $\partial B'$, and the case of almost maximal balls with two contacts of the second type at two coplanar edges of $\partial\Omega$ which are realized in the interior of *only one edge* of $\partial B'$, by assuming that Ω and B are in *general position*.

Similar to the discussion in the planar situation one may observe that an almost maximal ball B' with only two contacts that are realized at two *neighboring* entities (i.e., facets, edges, or vertices) of $\partial B'$ is not maximal, since it is possible to apply a uniform scaling with a center that is located in the intersection of the two contact entities.

2.4 Medial axis

We define the *medial axis* $\text{MA}(\Omega)$ as the union of the centers of all almost maximal balls associated with Ω . The *medial axis transform* $\text{MAT}(\Omega)$ additionally contains the information about the scaling of the almost maximal balls which are centered at the points of $\text{MA}(\Omega)$.

The medial axis of a *planar shape* Ω consists of bisector curves (edges) and trisector points (branching points). In the general (non-degenerate) case, three edges meet at a branching point.

Consider the case (L) of a piecewise linear metric. Here, some of the bisectors correspond to nested families of almost maximal balls, which share the same contacts of type 1 on the boundary. These bisectors will be called *jump edges*, since the maximal inscribed balls jump between the two extreme positions, see Fig. 2a. If we did not consider jump edges, using only truly maximal balls for the definition, the medial axis of a connected planar domain Ω would possibly consist of several disconnect components. Moreover, if we relaxed the assumption of the general position by allowing almost maximal balls with two contacts of type 1 in the interior of only one edge of $\partial B'$, these balls would produce *two-dimensional* components of the medial axis.

The medial axis of a *three-dimensional domain* Ω consists of bisector surfaces (sheets), trisector curves (seams) and junctions. In the generic case – meaning that there do not exist maximal balls with more than four contacts on the boundary of Ω – three sheets meet at a seam, and four seams meet at a junction point [13]. For the case (L), similar to the case of jump edges for planar domains, some of the sheets correspond to partially nested families of almost maximal balls. We will refer to them as *jump sheets*. Once again, these jump sheets – and consequently the consideration of almost maximal balls – are needed in order to guarantee that the medial axis of connected domains is again connected. By relaxing the assumption of general position one would obtain three-dimensional components of the medial axis, which do not occur in the Euclidean case and thus are clearly not desirable.

Proposition 1. *The medial axis in the case (L) is a piecewise linear structure.*

Proof. The bisectors of linear structures with respect to a piecewise linear metric or quasi-metric are again linear structures. The medial axis of a triangulated solid with respect to such a metric is composed of these bisectors and their intersections, which are also linear. \square

Another new phenomenon that occurs when using a piecewise linear metric (L) instead of the Euclidean one (E) is the implicit pruning of convex features

(edges or vertices) of the boundary, which are flat with respect to the unit ball, in the sense that a vertex of the unit ball fits into the wedge defined by the feature. Such features lead to the appearance of special branching points (see Fig. 2b) or seams, which we will call *pseudo-branchings* and *-seams*, respectively. The almost maximal balls centered there share only two points with the boundary of Ω . In the planar case, one of these contacts has to be of type vertex-vertex. In the 3D case, one of these contacts is of the type edge-vertex or vertex-edge.

We will come back to this issue in the next section.

3 Contacts and contact arrangements

In the next three sections we consider solely the case of piecewise linear metric (L) in three-dimensional space. All arguments are easily adaptable to the planar case.

3.1 Contacts

Recall that a ball B' is a scaled and translated copy of the polyhedral unit ball B . We shall denote the vertices, edges and facets of ∂B , $\partial B'$, and Ω uniformly as *components* of these boundaries.

For any boundary component x of B , we denote with x' its image under the restricted similarity transformation (translation and scaling) that maps B to B' . Moreover, for each boundary component x of ∂B we choose an arbitrary but fixed *representative* vertex $v = v(x)$, which is one of the three vertices of a triangle, one of the two end points of an edge, or the vertex itself in the case of a vertex.

Since we assumed that B and Ω are in general position, every boundary component (vertex, edge or facet) of an almost maximal ball shares at most one point with a component of $\partial\Omega$.

Definition 2 Consider an almost maximal ball B' and assume that the component y of $\partial\Omega$ has a common point with the component x' of B' . We say that the pair (x, y) is a *contact*.

The *regular* combinations of boundary components – which determine the structure of the medial axis – are vertex-facet contacts, edge-edge contacts and facet-vertex contacts. Even for objects and unit balls in general position, vertex-edge, edge-vertex and vertex-vertex contacts do occur, but they can be regarded as being *singular*. They define pseudo-structures of the medial axis, but do not induce any sheets or seams.

An almost maximal ball with *two* contacts is centered on a *sheet* of the medial axis, a ball with *three* contacts on a *seam* (cf. Fig. 3). An almost maximal ball centered on a *pseudo-seam* is also defined by *three* contacts, where two of these contacts are *adjacent*, meaning that the ball components, as well as the mesh components, are incident, respectively. As a consequence, the almost maximal

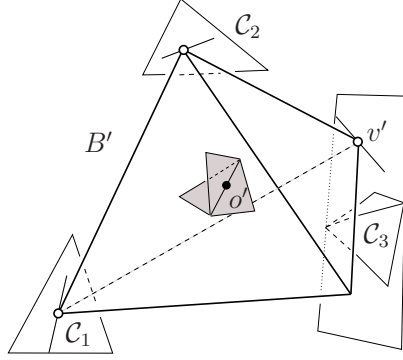


Fig. 3: The center o' of an almost maximal ball B' lies on a seam of the axis. The point v' is its projection on the contact plane of \mathcal{C}_3 .

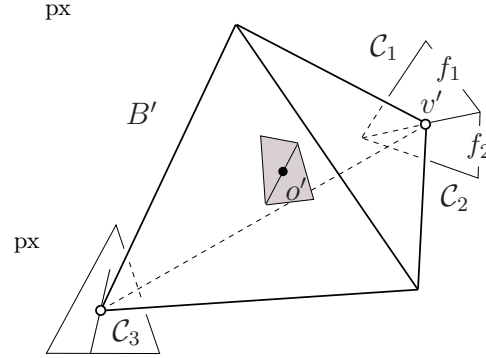


Fig. 4: The contact $\mathcal{C}_1 = (v, f_1)$ is adjacent to $\mathcal{C}_2 = (v, f_2)$. Consequently, the three contacts define a pseudo-seam containing o' .

ball's contact that is induced by these two adjacent contacts is, dependent on their types, of type vertex-edge or edge-vertex (see Fig. 4 for an illustration).

For every possible contact (x, y) the component $y \in \partial\Omega$ and the transformed ball component $x' \in B'$ span a plane, which will be called the *contact plane* associated with the contact.

3.2 Projections

An almost maximal ball B' possesses at least two contacts. Let $v(x)$ be the representative vertex of the ball part x of one contact (x, y) among them. We call v' , i.e., the equivalent of v on the translated and scaled copy B' of the unit ball B , the *projection* of the center o' into the contact plane of (x, y) .

Definition 3 Given a contact (x, y) , let $\mathcal{B}'(x, y)$ be the set of all almost maximal balls which realize this contact (x, y) . The set of all projections of the balls in $\mathcal{B}'(x, y)$ into the contact plane describes a polygonal region on the contact plane of (x, y) . We will call $\mathcal{D}(x, y)$ the *contact domain* of (x, y) .

A contact domain is the union of projections of medial axis components on the contact plane. As these components are piecewise linear, so are the projections on the plane and their union. Therefore a contact domain is a polygonal region.

Roughly speaking, the contact domain $\mathcal{D}(x, y)$ describes the trace of the representative vertex v for all almost maximal balls B' which share the contact (x, y) . For a vertex-facet contact (x, y) , the contact domain is contained in the mesh facet y , and there is only one contact with this facet. For the other non-singular types of contacts, the domain is contained in a plane containing

the boundary component, and there may be several contacts sharing a boundary component. A more detailed discussion will be given in [3]. The singular contacts (vertex-vertex, edge-vertex, and vertex-edge contacts) do not define a two-dimensional domain.

3.3 Contact arrangements

A seam of the medial consists of the center points o' of almost maximal balls B' that possess the same three contacts. For each of these three contacts (x, y) , the projections of the centers o' into the contact plane define a line segment on the contact plane, see Fig. 3. This line segment is contained in the contact domain $\mathcal{D}(x, y)$. In a similar way we obtain line segments that are projections of pseudo-seams.

The projections of all seams and pseudo-seams that share a given contact (x, y) form an arrangement of line segments, which we will call the *contact arrangement*, in the contact domain $\mathcal{D}(x, y)$.

Every edge of the contact arrangement represents a seam or a pseudo-seam. The junction points of the medial axis correspond to the vertices of the contact arrangement.

Remark 1. The medial axis may possess *jump sheets*, which correspond to partially nested families of almost maximal balls. While general sheets of the medial axis correspond to two-dimensional parts of the contact arrangements, the jump sheets may be represented by one-dimensional components (i.e., edges) as well, by choosing the representative vertex in a suitable way. Therefore, we need to treat jump sheets in a special way. This will be described in more detail in [3].

4 Computing the contact arrangements

As an almost maximal ball is implicitly defined by its contacts, the medial axis is fully represented by the contact arrangements. In order to analyze the medial axis, we compute the contact arrangements for all possible contacts (x, y) . Consequently, we reduce the problem of medial axis computation to a finite number of two-dimensional problems in the respective contact planes, which can moreover be addressed in parallel, since they are mutually independent.

4.1 Outline of the algorithm

For each contact (x, y) and its contact plane P , we perform the following algorithm, which is summarized visually in Fig. 5.

1. Create a stack of subdomains lying in P , and initialize it with the entire contact domain.
2. If the stack is empty, then continue with step 4, otherwise take a subdomain from the stack.

3. Check if there exists a seam or pseudo-seam which defines a projection line segment in P that hits the subdomain. If such a projection line is found, then split the subdomain along the line spanned by the segment into new subdomains and add them to the stack. Continue with the previous step.
4. Remove all line segments in the arrangement that do not represent projections of seams or pseudo-seams.

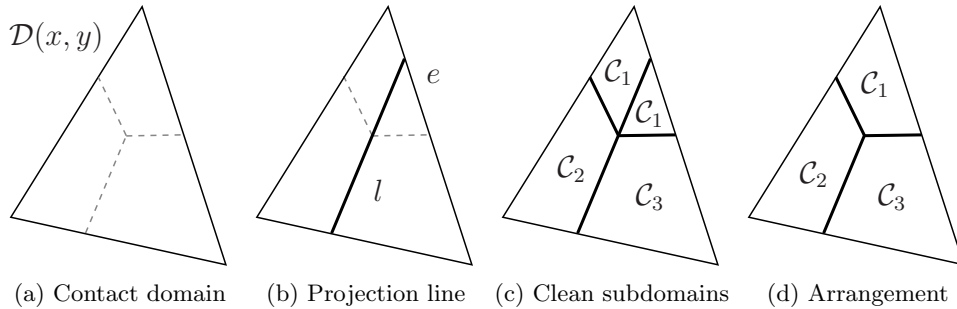


Fig. 5: Computation of a contact arrangement in a contact plane P .

4.2 Constructing almost maximal balls

Once again, let $v = v(x)$ be the representative vertex of the contact (x, y) . The most frequent (and also most expensive) operation of the algorithm is to compute an almost maximal ball B' for a point p on the contact domain, such that v' and p coincide. In particular, it is crucial to identify the remaining contacts of such an almost maximal ball. If there is only one additional contact, then p lies on a face of the contact arrangement, otherwise, it belongs to an edge.

An almost maximal ball is found by iterative shrinking, where p is the center of scaling. We start with a ball satisfying $p = v'$ which is sufficiently large to intersect the boundary mesh (see Fig. 6a). With help of an AABB (Axis Aligned Bounding Box) tree [4], the intersections between components of the ball boundary and the mesh are efficiently detected. The component of the mesh closest to p determines the shrinking factor. This is done iteratively until the shrunk ball and the mesh are intersection-free (see Fig. 6b). The last component of the mesh which is used to define the shrinking induces the second contact of the almost maximal ball. As all the above computations are done within the set of rational numbers, the resulting almost maximal ball and its center point are exact.

4.3 Finding projection lines

A projection line in the contact domain – which may be determined by a seam or a pseudo-seam – always corresponds to a change of the second contact of

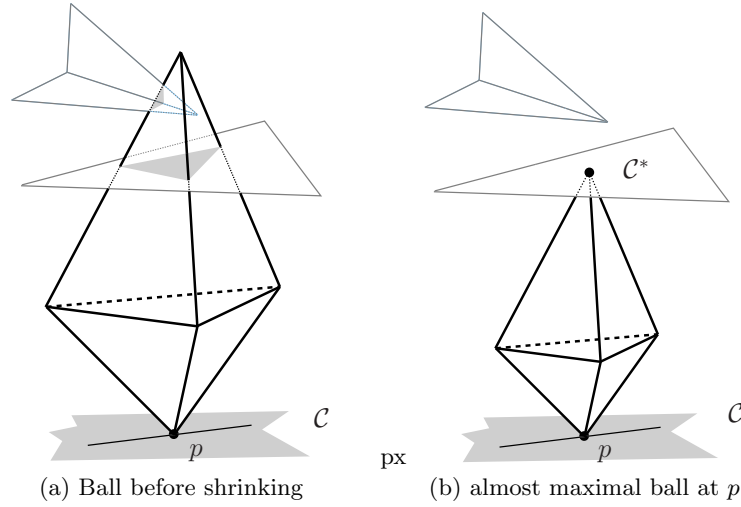


Fig. 6: Iterative computation of an almost maximal ball with a given projection p in a given contact plane (x, y) . The second contact is \mathcal{C}^* .

the associated almost maximal balls. Thus, the projection lines subdivide the contact domain into subdomains whose points define almost maximal balls with the same second contact.

Consider two points p and q on a contact domain. If the two associated almost maximal balls have different second contacts then we know that there exists a projection line crossing \overline{pq} . On the other hand, if the balls share the same opposite contact, then this does *not* imply that there is no such crossing line, since the faces of the contact arrangement are not necessarily convex.

If the associated second contacts \mathcal{C}_p and \mathcal{C}_q of p and q are different we need to find a point on the segment \overline{pq} which lies on a projection line. Roughly speaking, this is achieved by constructing a ball based on \overline{pq} and confined by the contact planes of \mathcal{C}_p and \mathcal{C}_q . If this ball turns out to be a valid almost maximal ball of Ω with three contacts, then its center lies on a seam or pseudo-seam and induces a projection line. Otherwise the interval between q and p is split and the search for two opposite contacts that define a projection line is continued iteratively by binary search. In non-singular configurations, this process is guaranteed to terminate.

On the other hand, in order to verify that no projection line crosses the edge \overline{pq} , where p and q have the same second contact, the family of almost maximal balls along \overline{pq} (which spans a convex polyhedron) has to be contained in Ω , see again [3] for more details. If the line segment \overline{pq} is not crossed by any projection line, then we call this segment *clean*. The final subdomains of the contact arrangement are characterized by the fact that they are bounded by clean segments.

4.4 Summary

For any given point on the contact domain we can construct the associated almost maximal ball. For two points on the domain we can decide if there exists a projection line that crosses the connecting segment of the points, and eventually find such a line. This is all we need to build the contact arrangement.

We start with the complete contact domain, and iterate over its boundary segments (Fig. 5a). If one of the segments induces a projection line, we split the domain at this line into two new subdomains and continue recursively (e.g., the edge e induces projection line l in Fig. 5b). If all boundary edges of a subdomain are *clean*, then the subdomain is *clean* and all points contained in it are associated with almost maximal balls having the same opposite contact, and thus lie on the same sheet of the axis (Fig. 5c). When all subdomains are clean we remove all artifact edges between neighboring subdomains describing the same sheet (two faces with opposite contact \mathcal{C}_1 are merged in Fig. 5d). This finally gives us the contact arrangement.

Remark 2. As said in Remark 1, a jump sheet may, depending on the representative vertex, correspond to a one-dimensional projection on a contact plane. Such a special *jump projection edge* is detected by an algorithm similar to the one for seams and pseudo-seams, which is, however, a bit more involved. For the computation of the contact arrangement such an edge is handled like any other projection line. For other representative vertices the jump sheet corresponds to a two-dimensional component (i.e., face) of the arrangement. In this case no *jump projection edge* occurs. For more details in this context see [3].

5 Assembling the medial axis and offset computation

Once we have computed all contact arrangements, the medial axis can be assembled by a simple algorithm. Based on this result we address the problem of trimmed offset computation. Finally we report experimental results that indicate the relation between the complexity of the input data (number of facets on $\partial\Omega$ and ∂B), the computing times and the size of the generated output.

5.1 Assembling the medial axis from its projections

When all contact arrangements are computed, the assembling of the axis can be performed by a simple computation. Any sheet of the axis is associated with two faces of two different contact arrangements, a seam with three edges of three arrangements. A pseudo-seam is induced by one arrangement edge, and two segments on the domain boundaries of two neighbored contacts. A jump sheet is associated with a *jump projection edge* or a face of a contact arrangement, depending on the representative vertex chosen for this contact. Every vertex of the arrangement is associated with an almost maximal ball B' , and the center points o' span the medial axis.

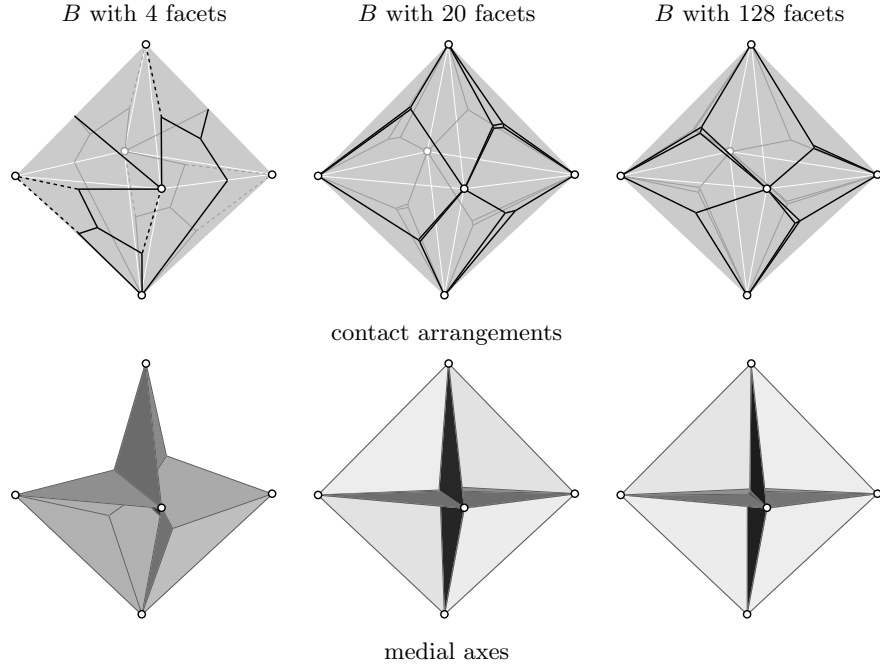


Fig. 7: Contact arrangements (top row) and medial axes (bottom row) of a slightly perturbed octahedron with respect to polyhedral unit balls with 4, 20 and 128 facets (from left to right). Dashed lines are projections of pseudo-seams.

The resulting medial axis is a non-manifold connected piecewise linear mesh. Connectivity can in general be derived from the contact arrangements. This means that two axis components are incident if their projections are incident in a contact arrangement. The *radial edge structure* introduced in [25] is one of several data structures that recommends itself for storing such a non-manifold mesh.

As a first example we consider a slightly perturbed octahedron Ω and compute its medial axis with respect to several polyhedral unit balls B , where the number of facets increases from 4 to 128. The results are shown in Fig. 7.

Since Ω is convex in this example, all contact domains are contained in the facets of Ω and only vertex-face contacts need to be considered. Consequently, the projections and contact arrangements can be visualized directly on $\partial\Omega$ (shown in the first row). The medial axis of the octahedron Ω with respect to the Euclidean unit ball consists of three squares which intersect each other along their diagonals. The medial axis with respect to a sparse polyhedral unit ball (a tetrahedron) is quite different (bottom left), since some of the vertices of the ball fit into the edge and vertex wedges of the domain. When using a polyhedral unit ball with a larger number of facets (bottom center and right), however, the structure of the computed medial axis is quite similar to the Euclidean case.

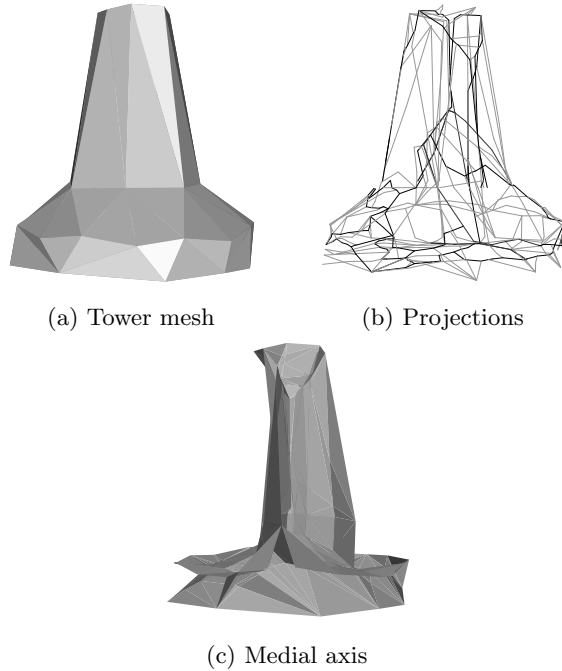


Fig. 8: Tower mesh, projections, and medial axis. The grey lines in (b) are the projections of pseudo-seams.

As a second example, we consider the “tower” object. Fig. 8 shows the object, the contact arrangements (projections) and the medial axis with respect to a piecewise linear quasi-metric generated by a tetrahedron. The mesh consists of 80 triangular facets and the resulting medial axis counts 269 sheets. As the object is non-convex, not all projections are realized directly on its boundary.

5.2 Offset Computation

The medial axis is a useful tool for trimmed offset computation. While this is well-established in the two-dimensional case [1, 8], the structure has not yet been used much in 3-space for this purpose [6].

The medial axis representation which is generated by our algorithm is directly useful for offset computation with respect to a linear (quasi-)metric. Each sheet \mathcal{S} of the medial axis is associated with two contacts \mathcal{C}_1 and \mathcal{C}_2 . An almost maximal ball B' with center point o' on \mathcal{S} and scaling factor s' has a unique point of contact p_i on \mathcal{C}_i for $i \in \{1, 2\}$. Let ρ be the offset size. Then the offset operation with ρ applied to B' gives us a new point p_i^ρ for each of the two contacts. This new point p_i^ρ lies on the line defined by p_i and o' . The position of p_i^ρ with respect to the sheet \mathcal{S} determines whether or not it has to be trimmed:

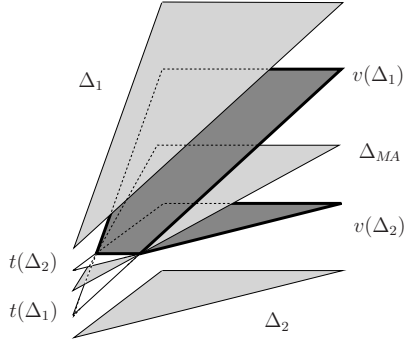


Fig. 9: The triangle Δ_{MA} of an axis sheet induces two triangles Δ_1 and Δ_2 on two different contact arrangements. The offset surface generated from each of these triangles is split into a valid ($v(\Delta)$) and a trimmed ($t(\Delta)$) part, which intersect in the corresponding axis sheet.

- If $s' > \rho$ then p_i^o lies between p_i and o' . Therefore p_i^o is a valid point of the offset surfaces.
- If $s' < \rho$ then o' lies between p_i and p_i^o . Therefore p_i^o has to be trimmed.
- If $s' = \rho$ then $p_1^o = p_2^o = o'$ and the point lies on the axis sheet where the trimmed and valid part of the offset surfaces are joined.

The axis sheets as well as the assigned faces of the contact arrangements are polyhedral regions. A triangulation on the sheet induces a triangulation on the faces, leaving us with a configuration as visualized in Fig. 9, where the three almost maximal balls at the corner points are known. Depending on the offset size ρ , certain parts of the triangles that lie on planes parallel to the contact planes define the valid offset surface. Note that a part derived from an edge-edge or facet-vertex contact resides on a plane which is partially defined by features of the unit ball.

We define the trimmed offset in 3D analogously to the planar one in [1]. It should be noted that the obtained offset is induced by the distance function d_{-B} , where $-B$ is the image of B under reflection at the origin o . Clearly, the two distance functions d_B and d_{-B} are identical for centrally symmetric unit balls B .

We performed the trimmed offset computation for the Armadillo mesh. A typical result is shown in Fig. 10.

5.3 Computing time and size of the medial axis

The time needed for the computation of the contact arrangements depends on various criteria. The quality of the boundary mesh influences the computing time gain provided by the AABB-tree structure. A rather complex and strongly branched shape has more reflex features and thus more edge-edge and facet-vertex contacts. On the other hand the nesting complexity of the single contact arrangements is in average higher for less ramified shapes, which also increases the computing time.

At this stage we cannot present any theoretical results. In order to obtain empirical data, we used several instances of the Armadillo mesh (see Fig. 10),

# faces	4	8	20	128
115	115.54	270.44	834.66	4645.03
267	284.04	594.75	1846.20	11770.50
575	525.19	1117.43	3011.68	21619.20
1396	1209.51	2120.49	6005.36	37837.30

Table 1: Computation times in seconds for different combinatorial sizes of B (rows) and different instances (columns) of the Venus model shown in Figure 14.

and tested it against various polyhedral unit balls (see Fig. 11). The computation times are reported in Fig. 12. They, as well as the ones provided in Table 1 for several instances of the “Venus”-shape, compare favorably with the ones reported in [13], which is the only implementation we are aware of that constructs the exact medial axis with respect to a specific metric. There, the computation of the medial axis for the “Venus”-shape with 250 faces is performed in 5.6 hours, with computing times growing considerably with respect to the number of faces. As can be seen in Table 1, we compute the exact medial axis with respect to the quasi-metric induced by a tetrahedral B for an instance with 267 faces (see Figure 14) in less than 5 minutes. Also, the computation times for the Armadillo and the Venus example grow only slightly super-linearly with respect to the number of facets of the mesh, and even sub-linearly with respect to the number of facets in the unit ball.

Finally we analyze the relation between the size (i.e., the number of planar sheets) of the computed medial axis and the number of facets on the boundaries of $\partial\Omega$ and of ∂B , see Fig. 13, again for the Armadillo example. The size of the medial axis grows linearly with the size of $\partial\Omega$, but only very slowly (much less than linear) with the size of ∂B . This will be analyzed in more detail in the future.

6 Convergence

The quasi-metric defined by a convex polyhedron B can be seen as an approximation of the Euclidean metric. Indeed, if the unit ball B converges to the Euclidean unit ball, then the quasi-metric defined by it converges to the Euclidean metric. The convergence of the unit balls can be described with the help of the Hausdorff distance. Recall that the Hausdorff distance of two sets X and Y is defined as

$$\text{HD}(X, Y) = \max\left(\sup_{x \in X} \inf_{y \in Y} \|x - y\|, \sup_{y \in Y} \inf_{x \in X} \|x - y\|\right). \quad (2)$$

In this section we consider simultaneously two metrics and the associated medial axes. On the one hand, we have the piecewise linear (quasi-) metric d_B defined by the convex polyhedron B and the medial axis $\text{MA}_B(\Omega)$ of the given domain Ω with respect to it. On the other hand, we have the usual Euclidean metric and the standard medial axis, which we will now denote with $\text{MA}(\Omega)$.

6.1 Planar domains

For planar domains $\Omega \subset \mathbb{R}^2$, the following result establishes a close connection between the two skeletal structures $\text{MA}_B(\Omega)$ and $\text{MA}(\Omega)$:

Theorem 1 *Consider a planar domain $\Omega \subset \mathbb{R}^2$ with piecewise linear boundary $\partial\Omega$. If the convex polygon B that serves as the unit ball of the (quasi-) metric d_B converges to the Euclidean unit circle, then the Hausdorff distance between the medial axes $\text{MA}_B(\Omega)$ and $\text{MA}(\Omega)$ with respect to the piecewise linear (quasi-) metric and the Euclidean metric, respectively, tends to zero.*

Thus, the convergence of the unit ball implies the convergence of the medial axis. Before proving this result we present the following result, which is visualized in Fig. 15.

Lemma 1. *Each point c' of the medial axis $\text{MA}_B(\Omega)$ of the planar domain Ω sees any two of its associated closest points on the boundary under a certain angle $\alpha'(c')$. For polygonal unit balls B that are sufficiently close to the Euclidean unit circle, there exists a lower bound φ' of this angle, which is independent of B . Each point c of the medial axis $\text{MA}(\Omega)$ sees any two of its associated closest points on the boundary under a certain angle $\alpha(c)$. There exists a lower bound φ of this angle.*

Proof. First we observe that none of the almost maximal polyhedral balls B' has a contact with the boundary of Ω in a convex vertex, provided that B is sufficiently close to the Euclidean unit circle. Similarly, none of the maximal Euclidean balls touches the boundary of Ω in a convex vertex. Consequently, each almost maximal polyhedral ball B' and each maximal Euclidean ball has contact

- with two edges of $\partial\Omega$ (both contacts are of type 1),
- with an edge and with a reflex (non-convex) vertex of $\partial\Omega$ (the contacts are of type 1 and type 2), or
- with two reflex vertices of $\partial\Omega$ (both contacts are of type 2).

Some balls may have more than two contacts, but we need to consider only two of them.

In the latter two cases, we consider the minimum distance d between any two reflex vertices and between any reflex vertex and any edge not starting or ending at this vertex. For all points c corresponding to these two types of contact, the angle $\alpha(c)$ satisfies $\alpha(c) \geq 2 \arcsin(d/D)$, where D is the diameter of Ω (which is also an upper bound on the diameter of the maximal Euclidean circles). Consequently, if B is sufficiently close to the Euclidean unit circle, the angle $\alpha'(c')$ satisfies $\alpha'(c') \geq \arcsin(d/D)$.

In the first case, the two contacts are realized at two non-parallel edges of $\partial\Omega$. Let β be the smallest angle between any two non-parallel edges of $\partial\Omega$. Here we consider all pairs of edges, not just the adjacent ones. For all points c corresponding to this type of contact, the angle $\alpha(c)$ satisfies $\alpha(c) \geq \beta$. Consequently, if B is sufficiently close to the Euclidean unit circle, the angle $\alpha'(c')$ satisfies $\alpha'(c') \geq \beta/2$. \square

Now we are ready to prove the convergence result.

Proof (Theorem 1). First we consider a point $c' \in \text{MA}_B(\Omega)$ and prove that there exists a point $c \in \text{MA}(\Omega)$ such that $\|c' - c\| \leq \varepsilon(B)$, where $\varepsilon(B)$ tends to zero as B converges to the Euclidean unit ball.

For a given $c' \in \text{MA}_B(\Omega)$ we consider the associated almost maximal ball B' , along with its inscribed circle and circumscribed circle. The almost maximal ball B' touches the boundary in at least two points $b', b'' \in \partial\Omega$, see Fig. 16a.

Consider the largest inscribed Euclidean ball with center c' . It touches the boundary $\partial\Omega$ at a point b , which is generally different from both b' and b'' . The boundary of this Euclidean ball lies between the inscribed circle and the circumscribed circle. The center c' sees b and one of the other two points – say b' – under an angle $\alpha > \frac{\varphi'}{2}$.

We consider the maximal inscribed Euclidean ball which is obtained by applying uniform scaling with center b and scaling factor $1+\delta$ to the ball with center c' , see Fig. 16b. This scaling maps the center c' into a new center c satisfying

$$\|c - c'\| = \delta\|c' - b\| \leq \delta D \quad (3)$$

where D is the diameter of the domain Ω . We find an upper bound on δ by considering the intersection p of the line segment from b to b' with the Euclidean circle with center c' . The uniform scaling moves this point towards b' , but not beyond b' , hence

$$\delta < \frac{\|p - b'\|}{\|p - b\|}, \quad (4)$$

cf. Fig. 17a. This upper bound on δ remains valid if the following operations are applied: First, we apply a uniform scaling with center c' and a scaling factor ≤ 1 which moves b and p to the inscribed circle. Second, we shift b' to the circumscribed circle along the line bb' . Third, the enclosed angle $\angle bc'b'$ is reduced to $\frac{\varphi'}{2}$, see Fig. 17b.

Let δ_0 be the upper bound on δ obtained after these operations, i.e., from the configuration in Fig. 17b. We can bound the distance $\|c - c'\|$ by $\varepsilon(B) = \delta_0(B)D$. Finally, if the polyhedral ball B converges to the Euclidean ball, then the distance between the inscribed and the circumscribed circle shrinks. Consequently, we obtain $\delta_0(B) \rightarrow 0$ and hence $\varepsilon(B) \rightarrow 0$.

In the second part of the proof we consider a point $c \in \text{MA}(\Omega)$ and prove that there exists a point $c' \in \text{MA}_B(\Omega)$ such that $\|c' - c\| \leq \varepsilon'(B)$, where again $\varepsilon'(B)$ tends to zero as B converges to the Euclidean unit ball. This can be proved by swapping the roles of circles and polyhedral balls with respect to the Euclidean and the piecewise linear metric, as follows.

For a given $c \in \text{MA}(\Omega)$ we consider the associated maximal Euclidean ball, along with its inscribed piecewise linear circle and circumscribed piecewise linear circle. This situation is visualized in Fig. 18a. The inscribed and circumscribed piecewise linear circles are shown as dashed polygons.

The inscribed piecewise linear circle possesses an inscribed Euclidean circle, and the circumscribed piecewise linear circle possesses a circumscribed Euclidean

circle. We will now refer to these two Euclidean circles as the inscribed circle and the circumscribed circle, respectively.

The maximal Euclidean ball with center c touches the boundary in at least two points $b', b'' \in \partial\Omega$, see Fig. 18a. Consider the largest inscribed piecewise linear ball with the same center c . It touches the boundary $\partial\Omega$ at a point b , which is generally different from both b' and b'' . The boundary of this Euclidean ball lies between the inscribed circle and the circumscribed circle. The center c sees b and one of the other two points – say b' – under an angle $\alpha > \frac{\varphi}{2}$.

Similar to the first part of the proof we consider the almost maximal inscribed piecewise linear ball which is obtained by applying uniform scaling with center b and scaling factor $1 + \delta'$ to the piecewise linear ball with center c , see Fig. 18b. This scaling maps the center c into a new center c' satisfying

$$\|c - c'\| = \delta' \|c - b\| \leq \delta' D. \quad (5)$$

As in the first part of the proof we are now able to construct an upper bound δ'_0 on δ' . If the polyhedral ball B converges to the Euclidean ball, then the distance between the inscribed and the circumscribed circle shrinks, which again implies $\delta'_0(B) \rightarrow 0$, and hence $\varepsilon'(B) \rightarrow 0$.

Finally, by combining the results of both parts we see that the Hausdorff distance of $\text{MA}(\Omega)$ and $\text{MA}_B(\Omega)$ tends to zero as B converges to the Euclidean unit ball. \square

Let h denote the Hausdorff distance between B and the Euclidean ball. The upper bounds δ_0 and δ'_0 can be bounded by Ch , where the constant C depends on the angles φ and φ' . Consequently, the Hausdorff distance of $\text{MA}(\Omega)$ and $\text{MA}_B(\Omega)$ is bounded by CDh . The constant C , however, is rather large for small values of φ and φ' .

6.2 Towards a convergence proof for the 3D case

In order to extend this approach to the spatial case, it is first necessary to analyze the possibility of generalizing Lemma 1. Unfortunately, for triangulated solids in 3D, it turns out that no such lower bound the angles α and α' exists in general.

If the piecewise linear ball is sufficiently close to the Euclidean one, then it suffices again to consider only piecewise linear balls that do not fit into any of the convex edges of the domain. Each almost maximal piecewise linear ball and each maximal Euclidean ball of Ω has contact

- with two facets of $\partial\Omega$, or
- with two entities of $\partial\Omega$, where at least one of them is a reflex edge or a non-convex vertex.

In the first case, a lower bound on the angles φ and φ' can be derived as in the planar case. In the second case, this is possible only if the two contact entities do not possess any common points.

More precisely, if the two entities which are present in the second case are two reflex edges with a common vertex, or a reflex edge and a facet possessing

a common vertex, then the technique used for proving the result in the planar case can no longer be applied, since it requires a lower bound on the distance between the two entities. Thus, a more sophisticated approach is required in order to generalize the convergence result to the 3D case.

We expect that the following approach allows to extend Theorem 1 to triangulated solids in space. First, we consider only the subset of the medial axes which are generated by almost maximal balls and by maximal Euclidean balls where the angle introduced in Lemma 1 exceeds a certain threshold ϕ^* . We denote these subsets by $\text{MA}_B^*(\Omega)$ and $\text{MA}^*(\Omega)$, respectively.

Next we consider a sequence $(B_n)_{n=1,2,\dots}$ of unit balls with the property that the ratio between the radii of the circumscribed and the inscribed ball has the upper bound $1 + 1/n^3$. For each of these balls we use the associated threshold $\phi_n^* = 1/n$ to define the subsets $\text{MA}_B^*(\Omega)$ and $\text{MA}^*(\Omega)$. Thus, after an appropriately scaling of B_n , the Hausdorff distance between the piecewise linear unit ball and the unit ball tends to zero as $1/n^3$, while the lower bound on the angle tends to zero as $1/n$.

Using the same techniques as in the proof of Theorem 1, we can conclude that the one-sided Hausdorff distances between $\text{MA}_B^*(\Omega)$ and $\text{MA}(\Omega)$ and between $\text{MA}^*(\Omega)$ and $\text{MA}_B(\Omega)$ converge to zero as $n \rightarrow \infty$. Simultaneously, the lower bound ϕ_n^* on the angle ϕ used for defining $\text{MA}_B^*(\Omega)$ and $\text{MA}^*(\Omega)$ tends to zero.

Finally, it should be possible to prove that the Hausdorff distances between $\text{MA}^*(\Omega)$ and $\text{MA}(\Omega)$, and between $\text{MA}_B^*(\Omega)$ and $\text{MA}_B(\Omega)$ converge to zero as well. The desired convergence result can then be obtained by combining these observations. The details of this proof cannot be described satisfactorily in the frame of this paper and will be reported elsewhere.

7 Concluding remarks

We have presented an algorithm which computes a piecewise linear medial axis representation $\text{MA}(\Omega)$ of a triangulated polyhedron Ω with respect to a piecewise linear quasi-metric d_B . The representation allows convenient trimmed offset computation, and all computations can be performed within the field of rational numbers. We would like to point out that the shape is not required to be simply connected, as the axis-representing contact arrangements are computed independently. This makes the algorithm easily accessible for parallel implementation. The algorithm shows convincing computational complexity and is suitable for larger meshes.

The complexity of the polyhedral unit ball can be chosen depending on the respective application. This is also one of the interesting issues for future research in this area. Given a mesh, what does a (preferably combinatorially small) polyhedral unit ball have to look like to reduce the occurrence of pseudo-seams? With a decreasing number of pseudo-seams, a combinatorial structure close to the Euclidean medial axis is to be expected. On the other hand the implicit pruning induced by the piecewise linear metric might be a welcome feature. This leads to the question how to locate points on the unit sphere, such that the vertices

of the resulting convex polyhedral ball enter as many flat convex features of a mesh as possible.

Modifications of the unit ball B do affect the geometric as well as the combinatorial appearance of $\text{MA}(\Omega)$. Another interesting task is to identify and isolate the combinatorially stable – and thus essential – parts of the medial axis by comparing the representations for different quasi-metrics d_B resulting from several different polyhedral unit balls B .

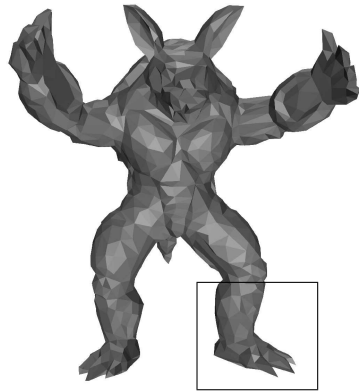
Acknowledgment

This research was supported by the Austrian Science Fund (FWF) through the National Research Network S92 “Industrial Geometry”, subprojects 2 and 5. The authors thank the reviewers for their comments which have helped to improve the paper.

References

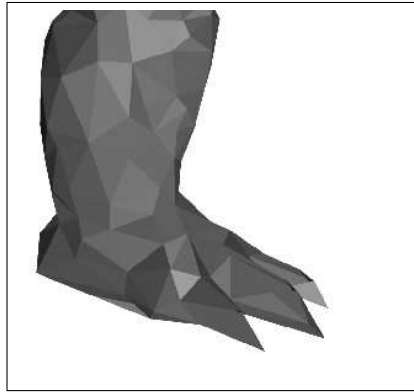
1. O. Aichholzer, W. Aigner, F. Aurenhammer, T. Hackl, B. Jüttler, E. Pilgerstorfer, and M. Rabl. Divide-and-conquer for Voronoi diagrams revisited. *Comput. Geom. Theory Appl.*, 43:688–699, October 2010.
2. O. Aichholzer, W. Aigner, F. Aurenhammer, T. Hackl, B. Jüttler, and M. Rabl. Medial axis computation for planar free-form shapes. *Comput. Aided Des.*, 41:339–349, May 2009.
3. W. Aigner. *Generalized representation of geometric objects in 2D and 3D*. PhD thesis, Graz University of Technology, 2011. In preparation.
4. P. Alliez, S. Tayeb, and C. Wormser. AABB Tree. In CGAL User and Reference Manual. CGAL Editorial Board, 2010.
5. D. Attali, J.-D. Boissonnat, and H. Edelsbrunner. Stability and computation of medial axes: a state of the art report. In B. Hamann T. Moeller and B. Russell, editors, *Mathematical Foundations of Scientific Visualization, Computer Graphics, and Massive Data Exploration*. Springer-Verlag, Mathematics and Visualization, 2007.
6. B. Bastl, B. Jüttler, J. Kosinka, and M. Lávička. Volumes with piecewise quadratic medial surface transforms: Computation of boundaries and trimmed off-sets. *Computer-Aided Design*, 42:671–679, 2010.
7. H. Blum. A transformation for extracting new descriptors of shape. In Weiant Wathen-Dunn, editor, *Models for the Perception of Speech and Visual Form*, pages 362–380. MIT Press, Cambridge, 1967.
8. L. Cao and J. Liu. Computation of medial axis and offset curves of curved boundaries in planar domain. *Comput. Aided Des.*, 40(4):465–475, 2008.
9. F. Chazal and A. Lieutier. The λ -medial axis. *Graph. Models*, 67:304–331, July 2005.
10. L.P. Chew, K. Kedem, M. Sharir, B. Tagansky, and E. Welzl. Voronoi diagrams of lines in 3-space under polyhedral convex distance functions. *J. Algorithms*, 29:238–255, November 1998.
11. F. Chin, J. Snoeyink, and C. A. Wang. Finding the medial axis of a simple polygon in linear time. In *Discrete Comput. Geom*, pages 382–391. Springer-Verlag, 1995.

12. J.-M. Chung and N. Ohnishi. Matching and recognition of planar shapes using medial axis properties, 2007.
13. T. Culver, J. Keyser, and D. Manocha. Exact computation of the medial axis of a polyhedron. *Comput. Aided Geom. Des.*, 21:65–98, January 2004.
14. T. K. Dey and W. Zhao. Approximating the medial axis from the Voronoi diagram with a convergence guarantee. *Algorithmica*, 38:179–200, October 2003.
15. H. Edelsbrunner, and E.P. Mücke. Simulation of simplicity: a technique to cope with degenerate cases in geometric algorithms. *ACM Trans. Graph.*, 9(1):66–104, 1990.
16. M. Etzion and A. Rappoport. Computing the Voronoi diagram of a 3-D polyhedron by separate computation of its symbolic and geometric parts. In *Proceedings Symposium on Solid Modeling and Applications*, pages 167–178. ACM, 1999.
17. H.N. Guroy and N.M. Patrikalakis. An automatic coarse and finite surface mesh generation scheme based on medial axis transform. part 1: algorithms. *Engineering with Computers*, 8:121–137, 1992.
18. C. Icking, R. Klein, N.-M. Lê, L. Ma, and F. Santos. On bisectors for convex distance functions in 3-space. In *In Proc. 11th Canad. Conf. Comput. Geom*, 1999.
19. J.L. Kelley and I. Namioka. *Linear Topological Spaces*. Springer, New York, 1976.
20. D.T. Lee. Medial axis transformation of a planar shape. *IEEE Trans. Pattern Analysis and Machine Intelligence*, 4:363–369, 1982.
21. Y.-G. Lee and Kunwoo Lee. Computing the medial surface of a 3-D boundary representation model. *Advances in Engineering Software*, 28:593–605, 1997.
22. B. Miklos, J. Giesen, and M. Pauly. Discrete scale axis representations for 3D geometry. *ACM Trans. Graph.*, 29:101:1–101:10, July 2010.
23. M. Ramanathan and B. Gurumoorthy. Interior medial axis transform computation of 3D objects bound by free-form surfaces. *Computer-Aided Design*, 42:1217–1231, 2010.
24. E.C. Sherbrooke, N.M. Patrikalakis, and E. Brisson. An algorithm for medial axis transform of 3-D polyhedral solids. *IEEE Trans. on Visualization and Computer Graphics*, 2:44–61, 1996.
25. K. Weiler. The radial-edge structure: A topological representation for non-manifold geometric boundary representations. *Geometric Modelling for CAD Applications*, 3–36, 1988.
26. W. A. Wilson. On quasi-metric spaces. *American Journal of Mathematics*, 53(3):pp. 675–684, 1931.



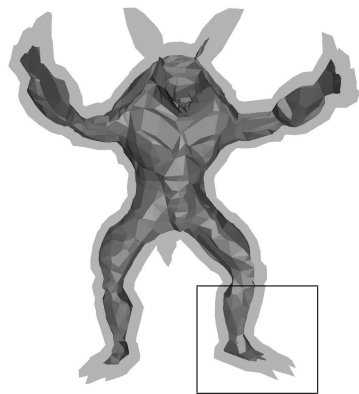
px

(a) Armadillo mesh with 3,124 facets



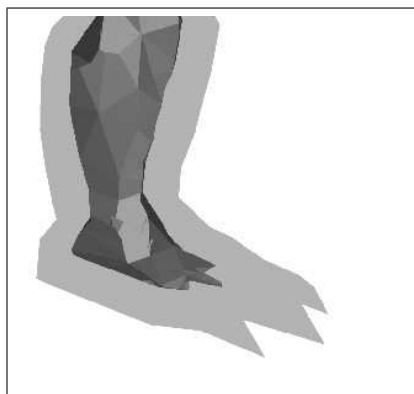
px

(b) Mesh detail



px

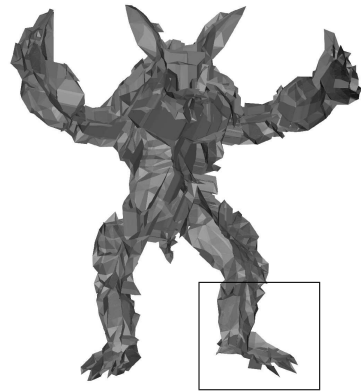
(c) Offset for tetrahedral B



px

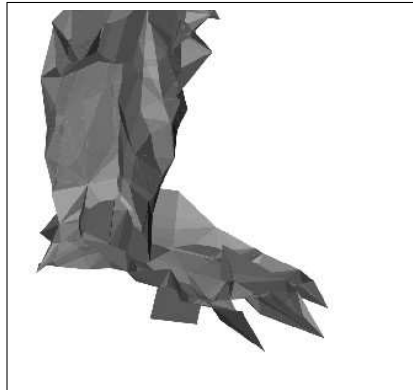
(d) Offset detail

Fig. 10: A version of the Armadillo mesh with 3124 facets and its trimmed offset for d_B with respect to a tetrahedral unit ball B .



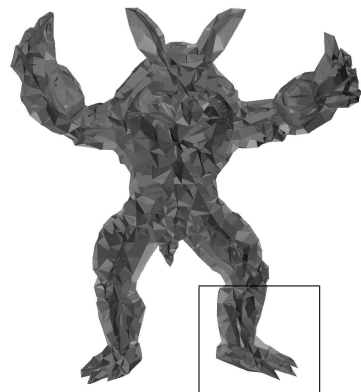
(a) B with 4 facets

px



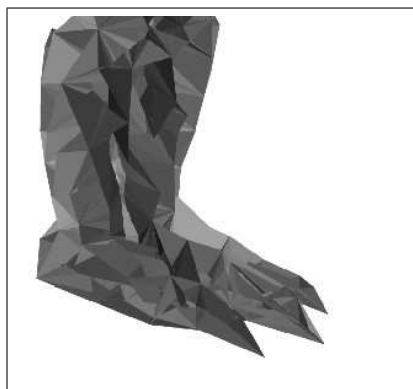
px

(b) Medial axis detail



(c) B with 128 facets

px



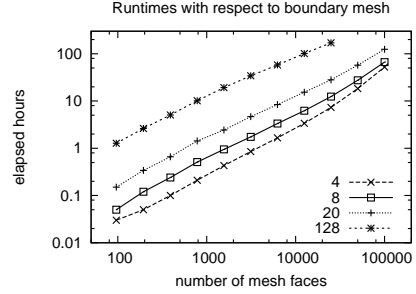
px

(d) Medial axis detail

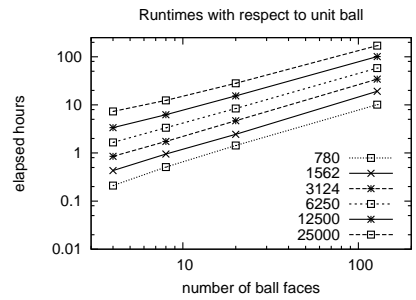
Fig. 11: The medial axis of the armadillo mesh from Fig. 10 for two different unit balls B .

# faces	4	8	20	128
96	0.03	0.05	0.15	1.28
194	0.05	0.12	0.34	2.63
390	0.10	0.24	0.66	5.05
780	0.21	0.51	1.43	10.13
1562	0.43	0.95	2.44	19.17
3124	0.85	1.74	4.67	34.24
6250	1.66	3.34	8.40	58.09
12500	3.37	6.23	15.39	101.12
25000	7.32	12.39	28.13	170.69
50000	18.28	27.46	57.38	-
100000	52.30	66.80	124.09	-

Fig. 12: Left: Computation times (in hours) for several polyhedral unit balls (shown in the different columns; the first row specifies the number of faces) and various instances of the Armadillo mesh (shown in the rows) on a single CPU with 2.5 GHz. Right: Results plotted on a log-log scale.



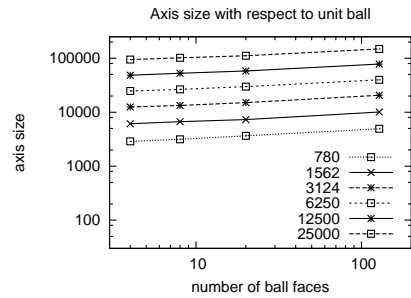
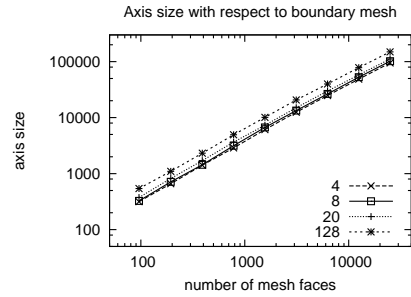
px pxpx



# faces	4	8	20	128
96	315	325	375	542
194	661	714	819	1097
390	1410	1437	1709	2315
780	2879	3154	3661	4945
1562	6106	6689	7316	10091
3124	12514	13365	15043	20655
6250	24764	26519	29841	39906
12500	48592	52655	58055	78155
25000	94715	101733	111355	148967

Fig. 13: Number of sheets of the medial axis for several polyhedral unit balls (shown in the different columns; the first row specifies the number of faces) and various instances of the Armadillo mesh (shown in the rows). Right: Results plotted on a log-log scale.

px



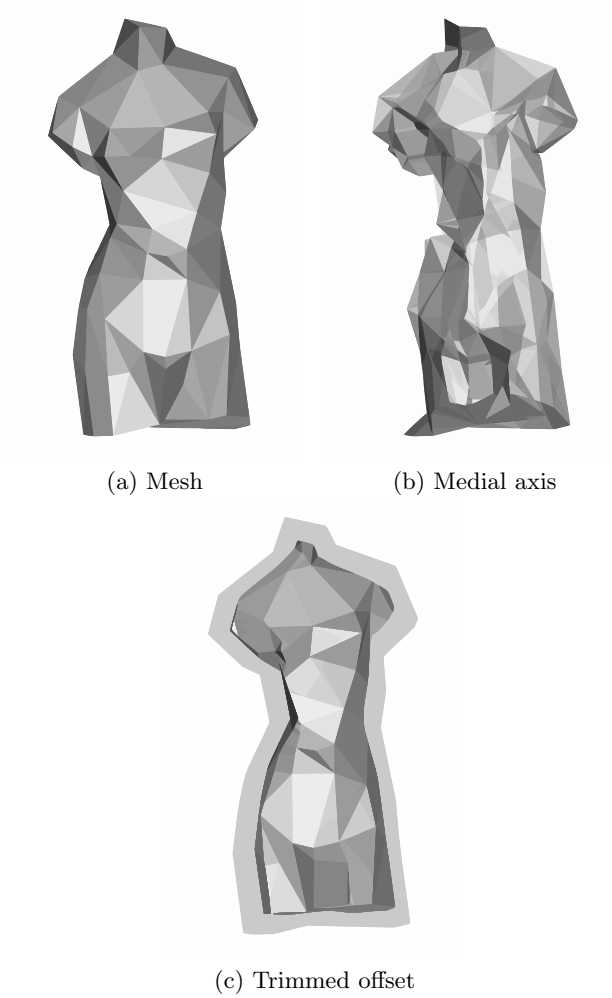


Fig. 14: (a) A mesh instance of the Venus model with 267 faces. (b) The medial axes induced by a unit ball B with 4 faces. (c) The resulting trimmed offset.

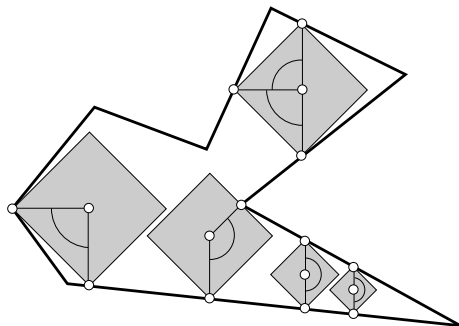


Fig. 15: Each center of a maximal (or almost maximal) ball sees any two of its associated boundary points under a certain angle. For piecewise linear boundaries, which are in general position with respect to the unit ball, this angle has a lower bound.

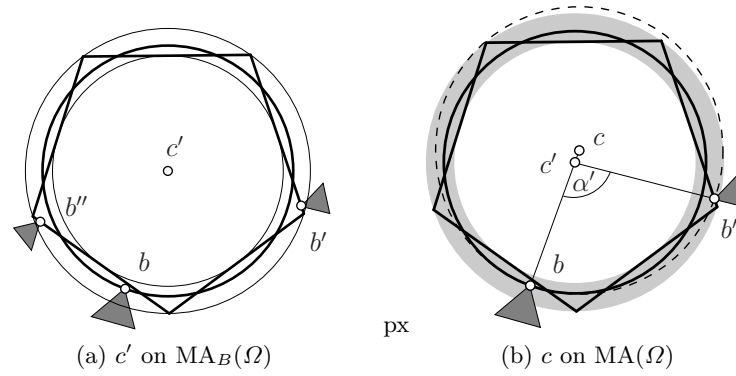


Fig. 16: The almost maximal polyhedral ball with center c' (left) and the construction of the associated maximal Euclidean ball (dashed) with center c (right).

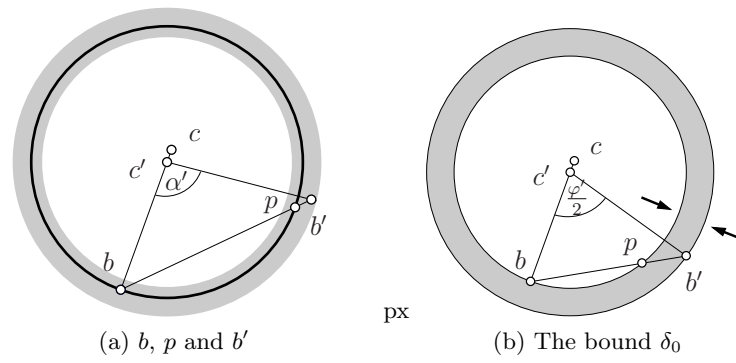


Fig. 17: The construction of an upper bound on the scaling factor $1 + \delta$.

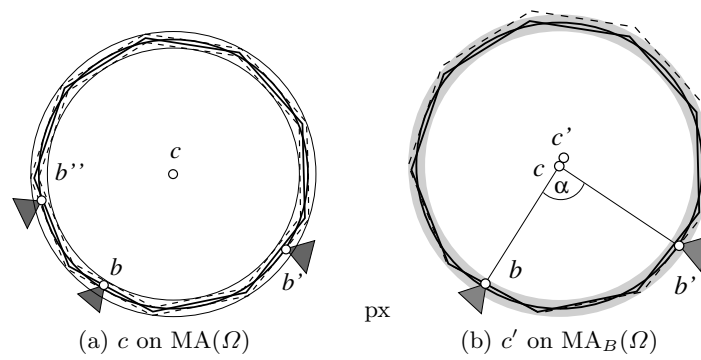


Fig. 18: The maximal Euclidean ball with center c (left) and the construction of the associated almost maximal polyhedral ball (dashed) with center c' (right).